Electrical contacts between cathodes and metallic interconnects in solid oxide fuel cells

Zhenguo Yang*, Guanguang Xia, Prabhakar Singh, Jeffry W. Stevenson

Pacific Northwest National Laboratory, Materials Science, 902 Battelle Blvd, P.O. Box 999, K2-44, Richland, WA 99352, USA

Abstract

In this work, simulated cathode/interconnect structures were used to investigate the effects of different contact materials on the contact resistance between a strontium doped lanthanum ferrite cathode and a Crofer22 APU interconnect. Among the materials studied, Pt, which has a prohibitive cost for the application, demonstrated the best performance as a contact paste. For the relatively cost-effective perovskites, the contact ASR was found to depend on their electrical conductivity, scale growth on the metallic interconnect, and interactions between the contact material and the metallic interconnect or particularly the scale grown on the interconnect. Manganites appeared to promote manganese-containing spinel interlayer formation that helped minimize the increase of contact ASR. Chromium from the interconnects reacted with strontium in the perovskites to form $SrCrO_4$. An improved performance was achieved by application of a thermally grown $(Mn,Co)_3O_4$ spinel protection layer on Crofer22 APU that dramatically minimized the contact resistance between the cathodes and interconnects.
© 2005 Elsevier B.V. All rights reserved.

Keywords: Solid oxide fuel cell; Interconnect; Electrical contact; Perovskite

1. Introduction

Solid oxide fuel cells (SOFCs) are solid-state energy conversion devices that produce electricity by electrochemically combining fuel and air across an ionic conducting electrolyte membrane. To build up a useful voltage, a number of cells are usually electrically connected in series in a "stack" via interconnects that also separate the fuel at the anode-side of one cell from the air at the cathode-side of the adjacent cell in planar SOFC stacks. One interconnection challenge facing SOFC developers is power loss within the stack due to high contact resistances between interconnects and cell electrodes [1–3]. To reduce electrode/interconnect interfacial resistances, electrical contact layers are often applied between the interconnects and electrodes during construction of a SOFC stack. For example, Ni paste in combination with Ni-mesh that is welded onto the metallic interconnects is widely used to establish electrical contact between metallic interconnects and YSZ/Ni anodes [4,5]. The use of nickel allows for establishment of a metallurgical bond between the Ni-containing anode and the metallic interconnect, providing a low electrical resistance path for electron transport across the anode–interconnect interface. In comparison, finding suitable materials for electrical contact layers at the cathode-side can be more challenging, particularly in intermediate temperature (600–800 °C) SOFCs where high-temperature oxidation-resistant alloys are used as interconnects [6–9]. At the cathode-side, as shown in Fig. 1, the contact layer connects a conductive cathode oxide (e.g. Sr-doped lanthanum ferrite, LSF, or Sr-doped lanthanum manganite, LSM) at one side and a metallic interconnect at the other. Therefore, there always exists a ceramic/metal interface, and possible additional ceramic/ceramic interfaces as well, all of which potentially contribute to a high contact resistance and thus a power loss. Accordingly, there is a pressing need for suitable contact materials to minimize the interfacial electrical resistance and maximize the power output of SOFC stacks.

* Corresponding author. Tel.: +1 509 375 3756; fax: +1 509 375 2186.
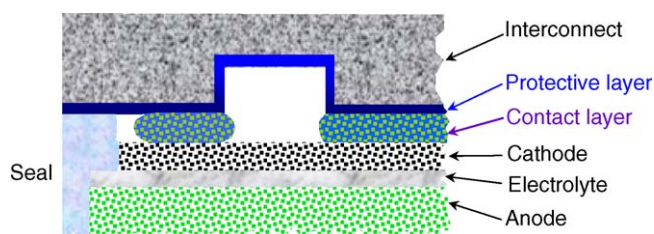 *E-mail address:* zgary.yang@pnl.gov (Z. Yang).

Fig. 1. Schematic illustration of a cathode–interconnect interface in an SOFC stack.

1.1. Contact resistance and materials requirements for electrical contacts

In this work, contact resistance is defined as the electrical resistance across an interconnect/electrode interface, specifically the metallic interconnect/cathode interface. Without a contact layer between a cathode and a metallic interconnect, the contact resistance rises from scale growth on the metallic interconnect, limited contact between the interconnect and cathode, and possible chemical interactions at the interface. With the use of an electrical contact layer, the contact resistance is dependent on:

(i) scale or scale growth on the interconnect, specifically its growth rate and conductivity,
(ii) contact or contact area between the contact layer and the scale,
(iii) resistance of the contact layer itself,
(iv) contact or contact area between the contact layer and the cathode,
(v) and interactions among the contact layer, the metallic interconnect and the cathode.

A higher electrical conductivity of the scale and contact materials, a larger contact area of the contact layer with the cathode and interconnect, and/or favorable reactions at the interfaces, can all contribute a lower contact resistance.

Thus, there are several basic requirements that must be met to obtain low, stable contact resistance. First, the contact material must have high electrical conductivity to minimize the resistance of the contact layer itself. Second, the oxide scale grown on the metallic interconnect should be as conductive as possible. Due to the insulating nature of alumina or silica, this requirement essentially eliminates the use of any alumina- or silica-forming alloys for construction of interconnects, or at least the interconnect active areas that are in contact with the cathodes. Accordingly, chromia-forming alloys are the preferred interconnect materials due to the semi-conducting nature of their chromia or chromia-rich scale [6–11]. Third, the contact materials must be chemically compatible with both the chromia-forming interconnects and the perovskite cathodes, which are commonly made from strontium doped lanthanum manganite, ferrite, or cobaltite-ferrite. Undesirable reactions which form phases with high electrical resistance or poor thermal expansion match can potentially increase contact resistance. On the

other hand, interfacial reactions may be beneficial if the reaction products offer high electrical conductivity and appropriate thermal expansion. Interfacial reactions can also potentially assist in preventing chromium migration from the chromia-forming interconnect into the cathode, which often causes a severe degradation in cell performance [12–15]. Possible routes to Cr mitigation include taking advantage of thermodynamically favorable reactions between the contact material and chromia or chromia vapor species [16,17], or reaction-formation of a thin layer that acts as barrier to chromium transport via solid state diffusion. Fourth, the contact material as well as its reaction products should demonstrate an appropriate thermal expansion behavior and high thermochemical and structural stability in the oxidizing cathode environment. Fifth, an appropriate sintering activity of contact materials at SOFC stack fabrication temperatures helps to increase contact area and thus decrease contact resistance. It should be noted, however, that excessive sintering may eliminate porosity in the contact layer and block air flow to the cathode/electrolyte interface, thus affecting cell performance. Finally, the contact material must be cost-effective. This requirement essentially prevents the use of expensive precious metals (e.g. Pt) and their alloys. Silver, however, is an exception due to its relative low price, but its high volatility and rapid thermal etching in hot air [18,19], as well as structural instability under simultaneous air and fuel dual exposures [20], may limit its use in SOFCs operating at relative high temperatures.

In the present study, several perovskites were investigated as potential contact materials. Results of the investigation of their electrical performance and chemical stability in relation to a ferritic stainless steel interconnect material are presented and discussed.

2. Experimental

Different contact materials were evaluated in a fixture (shown in Fig. 2) that simulates the interconnect-cathode structure in SOFC stacks. Approximately 15 μm thick, porous LSF layers, representing the cathodes, were fabricated onto both sides of a dense, 2 mm thick $La_{0.8}Sr_{0.2}FeO_3$ (LSF) substrate via screen printing of LSF ink and a subsequent sintering at 1250 °C in air. The LSF substrate with "cathodes" was then sandwiched symmetrically between two alloy coupons, representing the interconnects. The alloy used in this work is Crofer22 APU, a ferritic stainless steel that was developed by Forschungszentrum Julich for SOFC interconnect applications [21,22] and commercialized by ThyssenKrupp VDM. It has the following nominal composition (wt.%): 22.8 Cr, 0.45 Mn, 0.08 Ti, 0.06 La, 0.005 C, ≤0.03 P, ≤0.03 S, balance Fe.

As potential contact layer compositions, several perovskite compositions – $La_{0.8}Sr_{0.2}FeO_3$ (LSF), $La_{0.8}Sr_{0.2}MnO_3$ (LSM), $La_{0.8}Sr_{0.2}Co_{0.5}Mn_{0.5}O_3$ (LSCM), and $La_{0.8}Sr_{0.2}CoO_3$ (LSC) – were synthesized via a glycine-
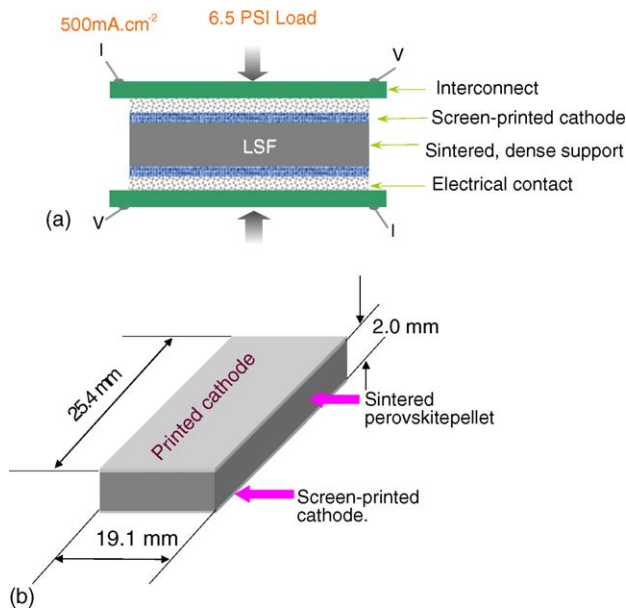
Fig. 2. Evaluation of interfacial electrical resistance at cathode material-interconnect material interfaces: (a) test setup; (b) dense $L_{0.8}S_{0.2}FeO_3$ pellet screen-printed with porous $L_{0.8}S_{0.2}FeO_3$ "cathodes" at both sides.

nitrate combustion synthesis process [23], and fabricated into pastes by mixing the powder with a binder (B-75717, Ferro Electric Materials) using a three-roll mill. The prepared paste was subsequently applied as contact layers between the Crofer22 APU coupons and LSF cathodes by screen-printing the contact paste onto the metal coupons and LSF cathodes. Pt was also tested as a reference contact layer material; submicron-size Pt paste was ordered from Ferro Electric Materials. During the tests, a dead load of 6.5 psi was uniformly applied onto the surface of Crofer22 coupons via an alumina plate in order to promote interfacial contact. A 4-point resistance technique was adopted to determine the resistance of the interconnect-cathode assembly. Platinum wire electrical leads were spot-welded onto the Crofer22 APU coupons using optimized parameters that give a stable metallurgical bonding between platinum wires and Crofer22 APU coupons [24]. A current density of $0.5\,A\,cm^{-2}$ was applied during the 800 °C test, while the voltage across the symmetrical test specimen was measured as a function of time. Each ASR test was duplicated at least once to verify reproducibility. The contact area-specific resistance (ASR) between the cathode and interconnect was obtained by dividing the measured ASR by two (due to the symmetrical test design). It should be noted that the contact ASR from this measurement includes the resistance of the LSF pellet and the porous cathode, which is estimated to be $\sim1.0\,m\Omega\,cm^2$ at 800 °C. ASR tests were performed with either bare Crofer22 APU or with Crofer22 APU covered with a thermally grown $Mn_{1.5}Co_{1.5}O_4$ protection layer. Details of preparation of the spinel protection layer can be found in Reference [25].

To investigate interfacial reactions between the interconnect and the contact materials, Crofer22 APU coupons were screen-printed with the paste of a selected material. After drying, the coated Crofer22 APU coupons were heat-treated at 800 °C in air for 300 h.

The samples from the ASR evaluation and reaction studies were sectioned and examined on a Philips XRG-3100 X-ray Generator with Cu Kα radiation and then under a JEOL scanning electron microscope (model 5900LV) equipped with energy-dispersive X-ray (EDX) capability at an operating voltage of 20 kV.

3. Results and discussion

3.1. Contact ASR of LSF||Crofer22 APU without and with Pt paste contact

To establish baseline performance data, the contact ASR of LSF||Crofer22 APU with no contact material, and with Pt paste as the contact material, was measured. As shown in Fig. 3(a), the use of Pt paste contact gave a contact ASR that was as low as $8.0\,m\Omega\,cm^2$ soon after the test temperature reached to 800 °C. The contact ASR then slowly increased to $8.6\,m\Omega\,cm^2$ after 180 h test, due to scale growth on the Crofer22 APU. The increase in ASR can be seen more clearly in the inlay figure in Fig. 3(a). In contrast, with no contact material present, the initial resistance started at $170\,m\Omega\,cm^2$, more than 20 times higher than that with the Pt paste contact, and increased to $235\,m\Omega\,cm^2$ after only 180 h. Obviously the poor contact between the Crofer22 APU and the LSF without contact paste led to the high initial ASR, while the use of the fine Pt paste promoted the contact between the alloy and LSF, thus dramatically decreasing the interfacial resistance. In addition to the difference in the initial ASRs, the rate of increase due to scale growth on the Crofer22 APU was also quite different. In the absence of a contact material, the interfacial ASR rose more quickly, especially in the early stages of the test, than with the Pt paste contact. The higher rate of ASR increase probably results from not only the increasing thickness of the scale grown on Crofer22 APU, but also a high contact resistance between the scale and LSF.

3.2. Contact ASR of LSF||Crofer22 APU with perovskite contacts

As mentioned, the high cost of Pt prohibits the use of Pt as a contact material in commercial SOFC stacks. Therefore, LSF, LSM, LSCM and LSC were selected and evaluated as contact materials. Fig. 3(b) shows the contact ASR of these perovskite contacts as a function of time. As expected, the contact made with LSC, which has the highest electrical conductivity among the four selected perovskites [26,27], gave the lowest initial ASR, while the contact made from LSF or LSM, both of which demonstrate a relative lower electrical conductivity, led to a higher initial ASR. All four ASR curves exhibit an increasing trend over time, but the rates of increase were not identical. For LSF, the contact ASR
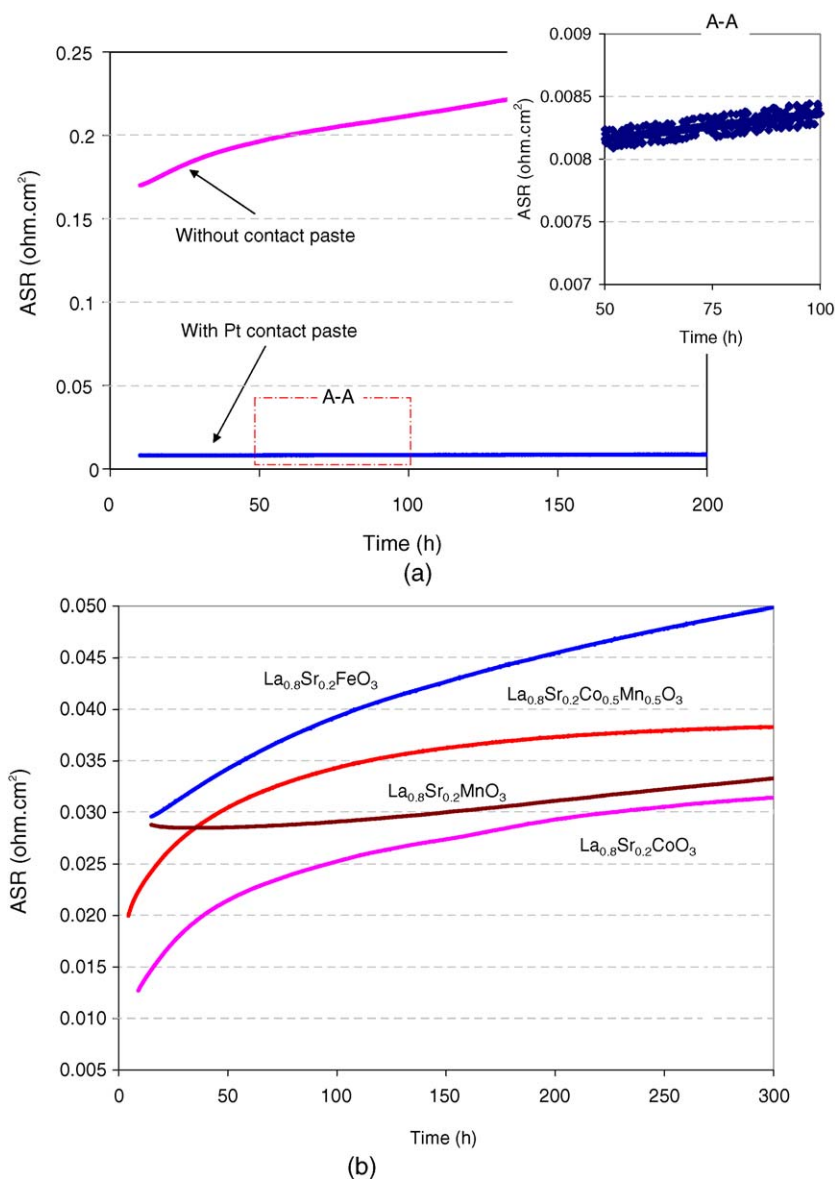
Fig. 3. Area specific resistance (ASR) for Crofer22 APU–$La_{0.8}Sr_{0.2}FeO_3$ interface as a function of time: (a) with Pt contact paste and with no contact paste; (b) comparison of ASR for Crofer22 APU||$La_{0.8}Sr_{0.2}FeO_3$ interface with $La_{0.8}Sr_{0.2}FeO_3$, $La_{0.8}Sr_{0.2}MnO_3$, $La_{0.8}Sr_{0.2}CoO_3$, and $La_{0.8}Sr_{0.2}Co_{0.5}Mn_{0.5}O_3$ contact paste.

increased quickly and steadily over the time span of the test. For LSC and LSCM, the contact ASR rose quickly initially and then increased more slowly during the rest of the test. The slowest rate of increase was observed for the LSM contact. The difference in the rates of increase of ASR is likely to result from interactions between the growing oxide scale and the contact materials. For example, the reaction between the LSM contact and the scale grown on Crofer22 APU promoted the formation of a spinel interlayer (to be discussed in Section 3) that likely acted as a mass transport barrier and inhibited the growth of the subscale, thus minimizing the increase of contact ASR.

The measurements described above used bare (i.e., unoxidized and unprotected) Crofer22 APU coupons. A test was also performed using Crofer22 APU coupons to which a $Mn_{1.5}Co_{1.5}O_3$ spinel protection layer had been applied [25]; for this test LSCM was selected as the contact material. Fig. 4 shows the contact ASR with the protected Crofer22 APU, in comparison with that with bare Crofer22 APU. The thermally grown spinel protection on Crofer22 APU led to a dramatic reduction in the contact resistance between LSF and Crofer22 APU. The reduction in the contact ASR is mainly attributed to: (i) the higher electrical conductivity of $(Mn,Co)_3O_4$ spinels compared to Cr_2O_3 or $(Mn,Cr)_3O_4$ [28–30], the two major components found in the scale grown on Crofer22 APU [24], (ii) a decreased rate of the sub-scale growth [25], and (iii) possibly improved chemical compatibility of the contact material with the spinel protection layer
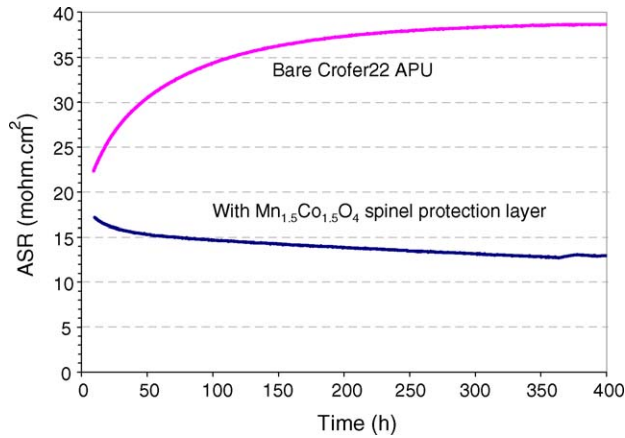
Fig. 4. Interfacial ASR for LSF and Crofer22 APU coated with $Mn_{1.5}Co_{1.5}O_4$ spinel as a function of time at $800\,°C$, compared with ASR for LSF and bare Crofer22 APU. $La_{0.8}Sr_{0.2}Co_{0.5}Mn_{0.5}O_3$ contact was used as the electrical contact material.

compared to its compatibility with Crofer22 APU or specifically the scale grown on the metal [30].

3.3. Interactions between Crofer22 APU and perovskite contact materials

As mentioned above, interactions between interconnects and contact materials can potentially have a significant effect on the magnitude and stability of the contact resistance. Therefore, the chemical compatibility between Crofer22 APU and the perovskite contact materials was also investigated. It was observed that manganese-containing perovskites, particularly LSM, facilitate the formation of manganese-containing spinels, e.g. $(Mn,Cr)_3O_4$, through reactions between the alloy scale and the manganite perovskites. As shown in Fig. 5(a), a thin interlayer was grown during oxidation in air at $800\,°C$. EDS mapping of Mn and Cr, as shown in Fig. 5(b and c), respectively, clearly revealed the enrichment of Mn and Cr in the interlayer, indicating likely formation of the $(Mn,Cr)_3O_4$ spinel via the interactions between LSM and Crofer22 APU and/or its scale. Previous studies [31,32] on interaction between $Cr5Fe1Y_2O_3$, a chromium-base interconnect alloy, and a manganite cathode also indicated the formation of $(Mn,Cr)_3O_4$ spinel at the interconnect and cathode interface. EDS point analysis at point "A" on the cross-section (see Fig. 5(a) and Table 1) found less than 0.5 wt.% Cr in the LSM layer. It appears that the manganite is more resistant to allowing Cr to displace Mn in the structure. Thus, in addition to the aforementioned role of minimizing the increase of contact ASR, the formed spinel interlayer also acted as a barrier to the Cr migration into the LSM coat. In contrast, a higher Cr concentration was observed in the ferrite and cobaltite (including LSCF and LSCM) that were coated on Crofer22 APU. As shown
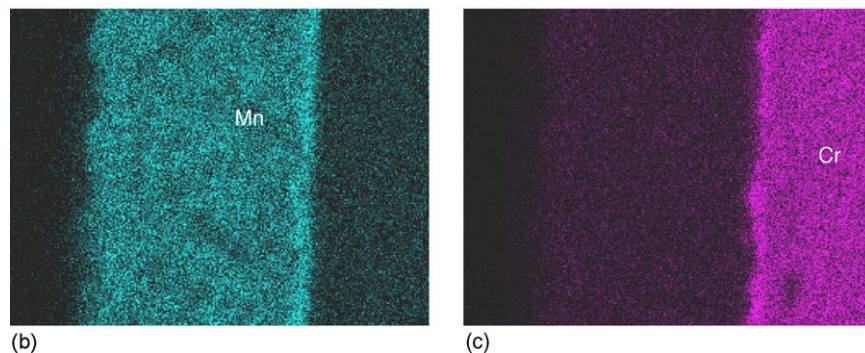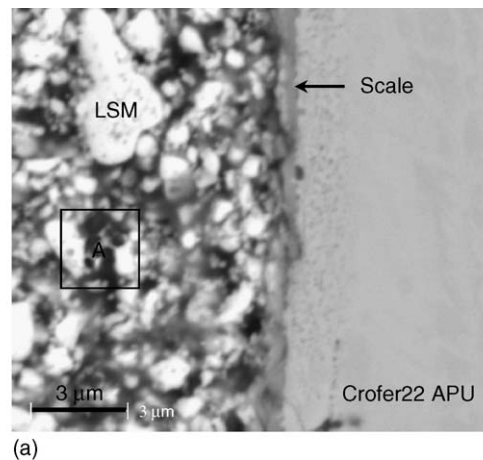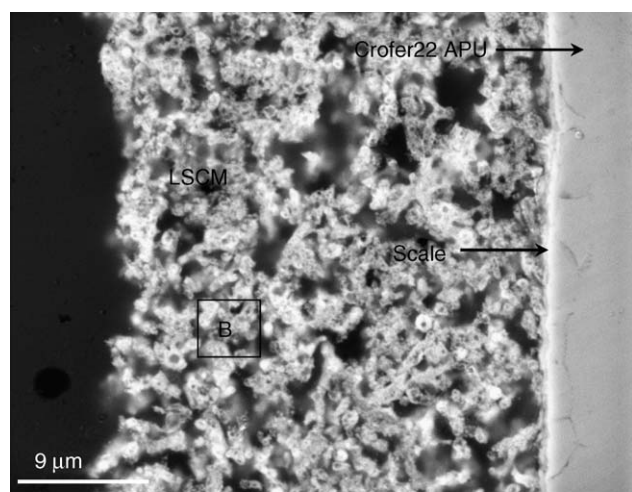

Fig. 5. Cross-section of Crofer22 APU with $La_{0.8}Sr_{0.2}MnO_3$ coating after heat-treatment at $800\,°C$ in air for 300 h: (a) SEM image of the cross-section; elemental maps of (b) Mn and (c) Cr.

Table 1
Chemical compositions of point "A", "B" and "C" in Figs. 5(a), 6(a) and (b), respectively

Elements (atomic%)	O	La	Sr	Fe	Co	Mn	Cr
A	33.53	26.02	7.46	0.52	–	31.55	0.91
B	19.93	26.26	7.83	1.12	21.39	13.39	10.08
C	39.97	22.27	5.05	26.26	–	0.58	5.85

in Fig. 6(b), EDS analysis at point "C" indicated 5.8 wt.% (refer Table 1) in the LSF layer after the 300 h heat treatment at 800 °C. An even higher Cr% was found in the cobaltite perovskite layers. For example, 10.8 wt.% Cr was found in the LSCM coat (see Fig. 6(a) and Table 1) after a similar heat treatment; in this case, the presence of manganese was not enough to block the migration of chromium into the perovskite coat. In other words, the cobaltite is more willing to incorporate the Cr than LSM. This result also indicates
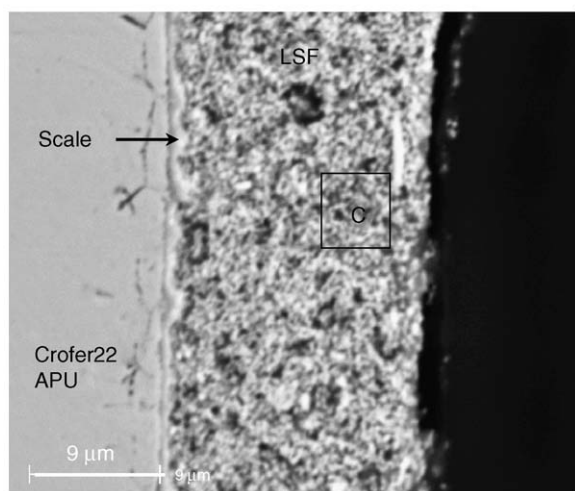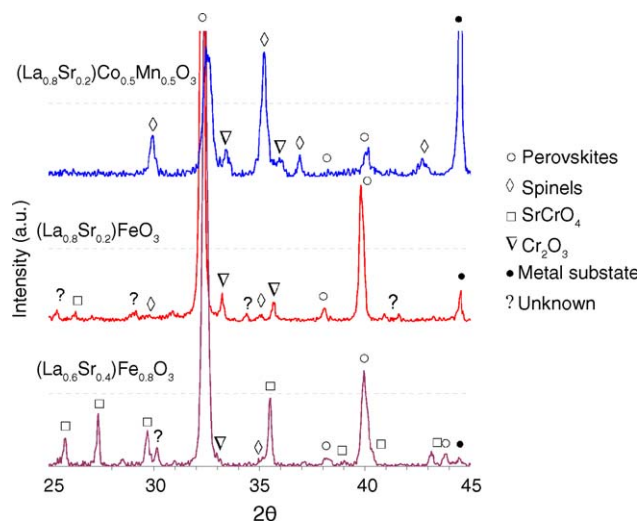
Fig. 7. XRD patterns of Crofer22 APU coupons with screen-printed $La_{0.8}Sr_{0.2}Co_{0.5}Mn_{0.5}O_3$, $La_{0.8}Sr_{0.2}FeO_3$, or $La_{0.8}Sr_{0.2}Co_{0.5}Mn_{0.5}O_3$ coatings, after heat-treatment at 800 °C in air for 300 h.

that a cobaltite contact layer can be a potential "getter" of chromium.

The X-ray diffraction study, as shown in Fig. 7, further confirmed the interaction between perovskites and the ferritic stainless steel, and helped identify the phases formed. For example, after 300 h at 800 °C, The M_3O_4 (M = Cr, Mn, Co) phase was obviously formed in the LSCM coating on Crofer22 APU. The XRD analysis also revealed the reaction of Sr from the perovskites with Cr from the alloy/scale to form $SrCrO_4$; this was especially the case for LSCF, which had 40at% Sr on the "A" site. This compound was also identified by others during their studies of interactions between strontium doped perovskites and chromia-forming alloys [31,33]. It is noted that there are still some unidentified peaks in the patterns, indicating the complexity of the materials systems. Also, it should be pointed out that, due to different element combinations and concentrations, variations in lattice parameters for a given crystal structure resulted in minor shifting of some XRD peaks.

4. Conclusions

ASR measurements under conditions that simulated the actual interfaces in SOFC stacks clearly indicated the need of electrical contact materials to promote the contact (and therefore minimize the contact resistance) between cathodes and metallic interconnects. An optimized contact material has to demonstrate high electrical conductivity, thermochemical and structural stability in the cathode environment, and good chemical compatibility with the cathode and interconnect materials.

Among different materials studied in the present work, Pt demonstrated the best performance as a contact paste. Its high cost, however, is expected to prevent its use as a

(a)

(b)

Fig. 6. SEM images of cross-sections of Crofer22 APU with (a) $La_{0.8}Sr_{0.2}Co_{0.5}Mn_{0.5}O_3$ or (b) $La_{0.8}Sr_{0.2}FeO_3$ coating after heat-treatment at 800 °C in air for 300 h.

contact material in commercial SOFC stacks. Perovskites, which are expected to be considerably lower in cost than Pt, exhibited contact ASRs that were initially determined primarily by the electrical conductivity of the contact material and initial contact between the cathodes and interconnects, while the changes as a function of time depended on the scale growth on the metallic interconnect and the interactions between the contact material and the metallic interconnect, or more specifically the scale grown on the interconnect. Manganites appeared to promote manganese-containing spinel interlayer formation that not only acted as a barrier to chromium migration but also help minimize the increase of contact ASR. Cobaltite contacts reacted and incorporated chromium that migrated from the chromia-forming interconnects. In particular, chromium from the interconnects reacted with strontium in the perovskite to form $SrCrO_4$. Overall the cathode/contact material/interconnect structures evaluated in the present study did not demonstrate sufficiently low ASRs for their applications in SOFC stacks. New contact materials and/or modification of existing contact materials or interconnects can result in improved performance. For example, as evidenced by the present study, a thermally grown $(Mn,Co)_3O_4$ spinel protection layer on Crofer22 APU dramatically minimized the contact resistance between the cathodes and interconnects.

Acknowledgements

References

[1] W. Schafer, A. Koch, U. Herold-Schmidt, D. Stolten, Solid State Ionics 86-88 (1996) 1235.

[2] S. Koch, P.V. Hendriksen, Solid State Ionics 168 (2004) 1.

[3] B. Bruckner, H. Landes, B. Rathjen, G.-S.-O. Fachhochschule, in: A. McEvoy (Ed.), Proceedings of the Fourth European Solid Oxide Fuel Cell Forum, vol. 2, The European SOFC Forum, Switzerland, 2000, p. 641.

[4] O. Teller, W.A. Meulenberg, F. Tietz, E. Wessel, W.J. Quadakkers, in: S.C. Singhal, H. Iwahara (Eds.), Proceedings of the Third International Symposium on Solid Oxide Fuel Cells, vol. 93-94, The Electrochemical Proceedings Series, Pennington, NJ, 1993, p. 641.

[5] M. Kuznecov, H. Greiner, M. Wohlfart, K. Eichler, P. Otschick, in: A. McEvoy (Ed.), Proceedings of the Fourth European Solid Oxide Fuel Cell Forum, vol. 2, The European SOFC Forum, Switzerland, 2000, p. 261.

[6] K. Huang, P.Y. Hou, J.B. Goodenough, Solid State Ionics 129 (2000) 237.

[7] W.J. Quadakkers, T. Malkow, J. Piron-Abellan, U. Flesch, V. Shemet, L. Singheiser, in: A. McEvoy (Ed.), Proceedings of the Fourth European Solid Oxide Fuel Cell Forum, vol. 2, The European SOFC Forum, Switzerland, 2000, p. 827.

[8] J. Piron-Abellan, V. Shemet, F. Tietz, L. Singheiser, W.J. Quadakkers, in: H. Yokokawa, S.C. Singhal (Eds.), Proceedings of the Seventh International Symposium on Solid Oxide Fuel Cells, vol. 2001-16, The Electrochemical Proceedings Series, Pennington, NJ, 2001, p. 811.

[9] Z. Yang, K.S. Weil, D.M. Paxton, J.W. Stevenson, J. Electrochem. Soc. 150 (2003) 1188.

[10] S.P.S. Badwal, R. Bolden, K. Foger, in: Ph. Stevens (Ed.), Proceedings of the Third European Solid Oxide Fuel Cell Forum, vol. 1, The European SOFC Forum, Switzerland, 1998, p. 105.

[11] T. Brylewski, M. Nanko, T. Maruyama, K. Przybylski, Solid State Ionics 143 (2001) 131.

[12] K. Hilpert, D. Das, M. Miller, D.H. Peck, R. Weiβ, J. Electrochem. Soc. 143 (1996) 3642.

[13] S.C. Paulson, V.I. Birss, J. Electrochem. Soc. 151 (2004) 1961.

[14] S. Taniguchi, M. Kadowaki, H. Kawamura, T. Yasuo, Y. Akiyama, Y. Miyaki, J Power Sources 55 (1995) 73.

[15] Y. Matsuzaki, I. Yasuda, J. Electrochem. Soc. 148 (2001) A126.

[16] C. Gindorf, L. Singheiser, K. Hilpert, Steel Res. 72 (2001) 528.

[17] C. Gindorf, L. Singheiser, K. Hilpert, M. Schroeder, M. Martin, H. Greiner, F. Richter, in: S.C., Singal, M., Dokiya (Eds.), Proceedings of the Sixth International Symposium on Solid Oxide Fuel Cells, vol. 99-19, The Electrochemical Society, Pennington, NJ, 1999, p. 774.

[18] B. Chalmers, R. King, R. Shuttleworth, Proc. R. Soc. A193 (1948) 465.

[19] E.D. Hondros, A.J.W. Moore, Acta Metall. 8 (1960) 647.

[20] P. Singh, Z. Yang, V. Viswanathan, J.W. Stevenson, J Mater. Eng. Perform. 13 (2004) 287.

[21] W.J. Quadakkers, V. Shemet, L. Singheiser, US Patent No. 2,003,059,335, 2003.

[22] J.P. Abeilan, V. Shemet, F. Tietz, L. Singheiser, W.J. Quadakkers, in: S.C. Singhal, M. Dokiya (Eds.), Proceedings of the Seventh International Symposium on Solid Oxide Fuel Cells, PV 2001-16, The Electrochemical Proceedings Series, Pennington, NJ, 2001, p. 811.

[23] L.A. Chick, L.R. Pederson, G.D. Maupin, J.L. Bates, L.E. Thomas, G.L. Exarhos, Mater. Lett. 10 (1990) 6.

[24] Z. Yang, J.S. Hardy, M.S. Walker, G. Xia, S.P. Simner, J.W. Stevenson, J. Electrochem. Soc. 151 (2004) 1825.

[25] Z. Yang, G. Xia, J.W. Stevenson, Electrochem. Solid State Lett. 8 (2005) A168.

[26] H.U. Anderson, Solid State Ionics 52 (1992) 33.

[27] J. Mizusaki, Solid State Ionics 52 (1992) 79.

[28] T. Sasamoto, N. Sumi, A. Shimaji, O. Yamamoto, Y. Abe, J. Mater. Sci. Soc. Jpn. 33 (1996) 32.

[29] A. Holt, P. Kofstad, Solid State Ionics 69 (1994) 137.

[30] Z. Yang, G. Xia, S.P. Simner, J.W. Stevenson, J. Electrochemical Soc., in press.

[31] W.J. Quadakkers, H. Greiner, M. Hansel, A. Pattanaik, A.S. Khanna, W. Mallener, Solid State Ionics 91 (1996) 55.

[32] S.P.S. Badwal, R. Deller, K. Foger, Y. Ramprakash, J.P. Zhang, Solid State Ionics 99 (1997) 297.

[33] T. Maruyama, T. Inoue, K. Nagata, in: S.C. Singhal, M. Dokiya (Eds.), Proceedings of the Seventh International Symposium on Solid Oxide Fuel Cells, PV 2001-16, The Electrochemical Proceedings Series, Pennington, NJ, 2001, p. 889.